Wavelength conversion and unicast of 10-Gb/s data spanning up to 700 nm using a silicon nanowaveguide

Noam Ophir,[1,*] Ryan K. W. Lau,[2] Michael Menard,[3] Xiaoliang Zhu,[1] Kishore Padmaraju,[1] Yoshitomo Okawachi,[2] Reza Salem,[4] Michal Lipson,[3,5] Alexander L. Gaeta,[2,5] and Keren Bergman[1]

[1]*Department of Electrical Engineering, Columbia University, New York, New York 10027, USA*
[2]*School of Applied and Engineering Physics, Cornell University, Ithaca, New York 14853, USA*
[3]*School of Electrical and Computer Engineering, Cornell University, Ithaca, New York 14853, USA*
[4]*PicoLuz LLC, Jessup, Maryland 20794, USA*
[5]*Kavli Institute at Cornell for Nanoscale Science, Cornell University, Ithaca, New York 14853, USA*
[*]*ophir@ee.columbia.edu*

Abstract: We report extremely large probe-idler separation wavelength conversion (545 nm) and unicast (700 nm) of 10-Gb/s data signals using a dispersion-engineered silicon nanowaveguide. Dispersion-engineered phase matching in the device provides a continuous four-wave-mixing efficiency 3-dB bandwidth exceeding 800 nm. We report the first data validation of wavelength conversion (data modulated probe) and unicast (data modulated pump) of 10-Gb/s data with probe-idler separations spanning 60 nm up to 700 nm accompanied with sensitivity gain in a single device. These demonstrations further validate the silicon platform as a highly broadband flexible platform for nonlinear all-optical data manipulation.

©2012 Optical Society of America

OCIS codes: (130.7405) Wavelength conversion devices; (190.4380) Nonlinear optics, four-wave mixing.

References and links

1. R. W. Tkach, "Scaling optical communications for the next decade and beyond," Bell Syst. Tech. J. **14**(4), 3–9 (2010).
2. A. Sano, H. Masuda, T. Kobayashi, M. Fujiwara, K. Horikoshi, E. Yoshida, Y. Miyamoto, M. Matsui, M. Mizoguchi, H. Yamazaki, Y. Sakamaki, and H. Ishii, "69.1-Tb/s (432 x 171-Gb/s) C- and extended L-band transmission over 240 Km using PDM-16-QAM modulation and digital coherent detection," in Optical Fiber Communication Conference, OSA Technical Digest (CD) (Optical Society of America, 2010), paper PDPB7.
3. H. C. H. Mulvad, M. Galili, L. K. Oxenløwe, H. Hu, A. T. Clausen, J. B. Jensen, C. Peucheret, and P. Jeppesen, "Demonstration of 5.1 Tbit/s data capacity on a single-wavelength channel," Opt. Express **18**(2), 1438–1443 (2010).
4. D. Qian, M. Huang, E. Ip, Y. Huang, Y. Shao, J. Hu, and T. Wang, "101.7-Tb/s (370×294-Gb/s) PDM-128QAM-OFDM transmission over 3×55-km SSMF using pilot-based phase noise mitigation," in National Fiber Optic Engineers Conference, OSA Technical Digest (CD) (Optical Society of America, 2011), paper PDPB5.
5. D. Hillerkuss, T. Schellinger, R. Schmogrow, M. Winter, T. Vallaitis, R. Bonk, A. Marculescu, J. Li, M. Dreschmann, J. Meyer, S. Ben Ezra, N. Narkiss, B. Nebendahl, F. Parmigiani, P. Petropoulos, B. Resan, K. Weingarten, T. Ellermeyer, J. Lutz, M. Möller, M. Hübner, J. Becker, C. Koos, W. Freude, and J. Leuthold, "Single source optical OFDM transmitter and optical FFT receiver demonstrated at line rates of 5.4 and 10.8 Tbit/s," in Optical Fiber Communication Conference, OSA Technical Digest (CD) (Optical Society of America, 2010), paper PDPC1.
6. J. Sakaguchi, Y. Awaji, N. Wada, A. Kanno, T. Kawanishi, T. Hayashi, T. Taru, T. Kobayashi, and M. Watanabe, "109-Tb/s (7x97x172-Gb/s SDM/WDM/PDM) QPSK transmission through 16.8-km homogeneous multi-core fiber," in Optical Fiber Communication Conference, OSA Technical Digest (CD) (Optical Society of America, 2011), paper PDPB6.
7. J. Hashimoto, K. Koyama, T. Katsuyama, Y. Iguchi, T. Yamada, S. Takagishi, M. Ito, and A. Ishida, "1.3 um travelling-wave GaInNAs semiconductor optical amplifier," in Optical Amplifiers and Their Applications, OSA Technical Digest Series (Optical Society of America, 2003), paper WB3.
8. Y. Nishida, M. Yamada, T. Kanamori, K. Kobayashi, J. Temmyo, S. Sudo, and Y. Ohishi, "Development of an efficient praseodymium-doped fiber amplifier," IEEE J. Quantum Electron. **34**(8), 1332–1339 (1998).
9. K. S. Wu, D. Ottaway, J. Munch, D. G. Lancaster, S. Bennetts, and S. D. Jackson, "Gain-switched holmium-doped fibre laser," Opt. Express **17**(23), 20872–20877 (2009).

10. B. Jalali, V. Raghunathan, D. Dimitropoulos, and O. Boyraz, "Raman-based silicon photonics," IEEE J. Sel. Top. Quantum Electron. **12**(3), 412–421 (2006).
11. S. Radic, C. J. McKinstrie, R. M. Jopson, J. C. Centanni, Q. Lin, and G. P. Agrawal, "Record performance of parametric amplifier constructed with highly nonlinear fibre," Electron. Lett. **39**(11), 838–839 (2003).
12. Y. Zhang, Y. Gu, C. Zhu, G. Hao, A. Li, and T. Liu, "Gas source MBE grown wavelength extended 2.2 and 2.5 μm InGaAs PIN photodetectors," Infrared Phys. Technol. **47**(3), 257–262 (2006).
13. F. Gholami, S. Zlatanovic, E. Myslivets, S. Moro, B. Kuo, C. Brès, A. Wiberg, N. Alic, and S. Radic, "10Gbps parametric short-wave infrared transmitter," in Optical Fiber Communication Conference, OSA Technical Digest (CD) (Optical Society of America, 2011), paper OThC6.
14. A. Bogoni, X. Wu, S. Nuccio, J. Wang, and A. Willner, "640Gbit/s reconfigurable OTDM add-drop multiplexer," in Optical Fiber Communication Conference, OSA Technical Digest (CD) (Optical Society of America, 2011), paper OMK4.
15. E. Tangdiongga, Y. Liu, H. de Waardt, G. D. Khoe, A. M. Koonen, H. J. Dorren, X. Shu, and I. Bennion, "All-optical demultiplexing of 640 to 40 Gbits/s using filtered chirp of a semiconductor optical amplifier," Opt. Lett. **32**(7), 835–837 (2007).
16. J. Van Erps, J. Schröder, T. D. Vo, M. D. Pelusi, S. Madden, D. Y. Choi, D. A. Bulla, B. Luther-Davies, and B. J. Eggleton, "Automatic dispersion compensation for 1.28Tb/s OTDM signal transmission using photonic-chip-based dispersion monitoring," Opt. Express **18**(24), 25415–25421 (2010).
17. C. Koos, P. Vorreau, T. Vallaitis, P. Dumon, W. Bogaerts, R. Baets, B. Esembeson, I. Biaggio, T. Michinobu, F. Diederich, W. Freude, and J. Leuthold, "All-optical high-speed signal processing with silicon–organic hybrid slot waveguides," Nat. Photonics **3**(4), 216–219 (2009).
18. M. A. Foster, A. C. Turner, J. E. Sharping, B. S. Schmidt, M. Lipson, and A. L. Gaeta, "Broad-band optical parametric gain on a silicon photonic chip," Nature **441**(7096), 960–963 (2006).
19. A. C. Turner-Foster, M. A. Foster, R. Salem, A. L. Gaeta, and M. Lipson, "Frequency conversion over two-thirds of an octave in silicon nanowaveguides," Opt. Express **18**(3), 1904–1908 (2010).
20. R. Salem, M. A. Foster, A. C. Turner, D. F. Geraghty, M. Lipson, and A. L. Gaeta, "Signal regeneration using low-power four-wave mixing on silicon chip," Nat. Photonics **2**(1), 35–38 (2008).
21. A. Biberman, B. G. Lee, A. C. Turner-Foster, M. A. Foster, M. Lipson, A. L. Gaeta, and K. Bergman, "Wavelength multicasting in silicon photonic nanowires," Opt. Express **18**(17), 18047–18055 (2010).
22. H. Hu, H. Ji, M. Galili, M. Pu, H. Hansen Mulvad, L. Oxenløwe, K. Yvind, J. Hvam, and P. Jeppesen, "Silicon chip based wavelength conversion of ultra-high repetition rate data signals," in National Fiber Optic Engineers Conference, OSA Technical Digest (CD) (Optical Society of America, 2011), paper PDPA8.
23. H. Ji, M. Pu, M. Galili, L. K. Oxenlowe, K. Yvind, J. M. Hvam, and P. Jeppesen, "Optical waveform sampling and error-free demultiplexing of 1.28 Tb/s serial data in a nanoengineered silicon waveguide," J. Lightwave Technol. **29**(4), 426–431 (2011).
24. N. Ophir, J. Chan, K. Padmaraju, A. Biberman, A. C. Foster, M. A. Foster, M. Lipson, A. L. Gaeta, and K. Bergman, "Continuous wavelength conversion of 40-Gb/s data over 100 nm using a dispersion-engineered silicon waveguide," IEEE Photon. Technol. Lett. **23**(2), 73–75 (2011).
25. J. B. Driscoll, Xiaoping Liu, J. I. Dadap, W. M. J. Green, Y. A. Vlasov, G. M. Carter, and R. M. Osgood, "All-optical format conversion of NRZ-OOK to RZ-OOK in a silicon nanowire utilizing either XPM or FWM and resulting in a receiver sensitivity gain of ~2.5 dB," IEEE J. Sel. Top. Quantum Electron. **16**(1), 234–249 (2010).

1. Introduction

The rapid growth in data traffic across telecom and metro-area networks, showing a persistent exponential increase of 60% per year [1], requires continued development of optical communication technologies to facilitate greater-bandwidth networking. Multiple recent research efforts aimed at increasing link bandwidth up to 100 Tb/s have emerged by utilizing massive wavelength division multiplexing (WDM) [2], optical time-division multiplexing (OTDM) [3], coherent modulation schemes [4], orthogonal frequency division multiplexing (OFDM) [5], and spatial parallelism in fibers [6]. However, most of this work has focused on the commercial telecom wavelength bands centered at 1.55 μm, spanning less than 100 nm of available optical spectrum. While erbium-based amplification and low-loss optical fiber have enabled extremely efficient operation within these wavelength bands, consideration should be given to operation at wider spectral bands, especially for potentially enhancing communication bandwidth.

The notion of operating outside the standard telecom bands is further strengthened by the introduction of fibers, amplifiers, and receivers at both longer and shorter wavelengths. Novel gain platforms operating at many different wavelength bands have emerged over the past few years such as semiconductor-optical amplifiers (SOAs), amplifiers that utilize rare-earth doped fiber such as praseodymium-, thulium-, and holmium, Raman amplifiers, and parametric amplifiers using highly nonlinear media [7–11]. While guiding, amplification, and detection [12] of light are possible over the full 1200 – 2000 nm wavelength range, device

performance in significant portions of this spectrum are still inferior to the well optimized devices within the telecom bands. One approach to bridge this performance gap between the different bands is to utilize broadband wavelength converters to effectively export capabilities from the telecom bands to other wavelength regions.

All-optical processing of high-speed data has been previously demonstrated on a wide range of platforms such as highly-nonlinear fibers, periodically-poled $LiNbO_3$ (PPLN), SOAs, chalcogenides, and silicon-organic hybrid waveguides [13–17]. Silicon nanowaveguides in particular present a very interesting platform for wavelength conversion as well as other all-optical functionalities based on four-wave mixing (FWM). Crystalline silicon's inherently high nonlinear response combined with tight mode confinement result in an effective nonlinear coefficient γ around 5 orders of magnitude larger than standard silica fiber [18]. Furthermore, tight modal confinement in the device not only enhances the effective nonlinearity, but also enables dispersion engineering through the tailoring of nanowaveguide dimensions. Combined with very short device length (several cm's), very broad phase matching is attainable, resulting in continuous 3-dB FWM bandwidth greater than 800 nm [19]. Finally, the complementary-metal-oxide-semiconductor (CMOS)-compatibility of these devices make the silicon nanowaveguides an ideal prospect for repeatable mass-production of very low-footprint low-cost devices, as well as enabling close integration with electronics. As FWM in silicon is virtually bit-rate and format transparent it can facilitate multiple all-optical data functionalities such as signal regeneration [20], multicasting [21], wavelength conversion [22], and demultiplexing [23] at symbol rates even greater than 1 Tbaud/s, with both on-off keyed [20,21,23] and phase-modulated data [22], but to date these functionalities have been data-measurement validated in silicon with only up to 100-nm probe-idler separations [24].

In this manuscript we report three distinct experimental demonstrations with a common goal of performing bit-error-rate (BER)-validation of silicon nanowaveguide FWM-based all-optical manipulation of 10-Gb/s data across very large probe-idler separations. In a first experiment we wavelength-convert the data across several discrete probe-idler separations, gradually stepping from 60 nm up to 168 nm to investigate device performance vs. probe-idler separation. In a second experiment we extend the conversion range by modifying the experimental setup to realize a 545-nm wavelength conversion of data, showing consistent performance compared with the first experiment. In both experiments, a high-repetition rate pulsed pump is used, creating format conversion of the data from Non-Return-to-Zero (NRZ) data at the probe wavelength to Return-to-Zero (RZ) data at the idler wavelength, resulting in a sensitivity gain (negative power penalty) at the receiver, consistent with other reported results [25]. Finally, in a third experiment we demonstrate the unicast functionality (pump modulated with data creating a copy of the data on the idler) with 700-nm probe-idler separation. In this case sensitivity gain is obtained through signal regeneration of the RZ pump data. Error-free operation (BER < 10^{-12}) is observed for all 10-Gb/s idler signals.

2. Experiments and measurements

2.1 Dispersion-engineered silicon nanowaveguide

The device used for these demonstrations (Fig. 1(a) inset) was fabricated at the Cornell Nanofabrication Facility using e-beam lithography followed by reactive ion etching. The oxide-clad silicon nanowaveguide is 1.1-cm long with a 300-nm by 710-nm core cross section surrounded by a 30-nm silicon slab. Device dimensions are designed to yield a zero-group-velocity dispersion (ZGVD) wavelength in the C-band. The ZGVD wavelength was estimated to be ~1546.5 nm, by optimizing the pump position to yield maximal FWM bandwidth. Inverse tapers on both facets provide efficient coupling to fiber. The device is laid out in a compact spiral occupying less than 1 mm^2 and has a 8.4-dB fiber-to-fiber loss. Two-photon absorption (TPA) and TPA-induced free carrier absorption result in 2-dB additional nonlinear loss when a 19-dBm optical pump is launched onto the waveguide.
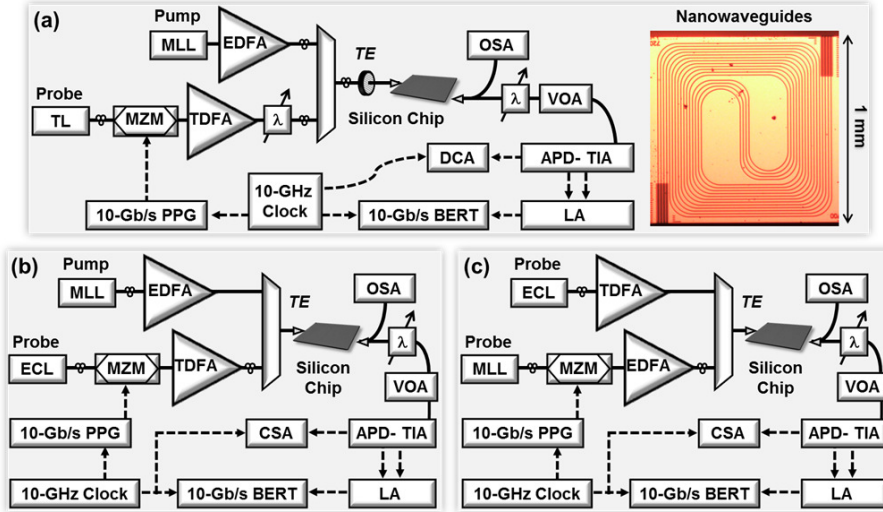
Fig. 1. Data-validation experimental setups for (a) Wavelength and format-conversion up to 168 nm with an inset of optical microscope image of four silicon nanowaveguides in a spiral layout; (b) Wavelength and format conversion at a 545-nm probe-idler separation; and (c) Unicast of a 10-Gb/s RZ signal with a 700-nm probe-idler separation.

2.2 Wavelength and format conversion up to 168 nm

The experimental setup (Fig. 1(a)) for this set of measurements includes a continuous-wave (CW) tunable laser (TL) whose output is on-off-keyed modulated by a commercial LiNbO$_3$ Mach-Zehnder modulator (MZM) with a 2^{31}-1 pseudo-random-bit-sequence (PRBS) pattern. The modulated light is amplified by an S-band thulium-doped fiber amplifier (TDFA) before being filtered (λ) and combined with a pulsed pump using a band combiner. The 1.5-ps, 10-GHz repetition-rate pump (located at 1555 nm) is generated by amplifying the output of a mode-locked-laser (MLL) by an erbium-doped fiber amplifier (EDFA). The combined signals are set to TE polarization and launched into the nanowaveguide. The nanowaveguide's output is filtered by a band filter to allow reception of the converted signal on a 10.7-GHz bandwidth InGaAs avalanche-photo-diode (APD-TIA). A variable optical attenuator is included before the receiver to facilitate measurement of BER curves. The output of the receiver is electrically amplified by a limiting amplifier (LA) before being evaluated on a bit-error-rate tester (BERT). A 40-GHz digital communications analyzer (DCA) is used to record the eye diagrams from the photodetector's output, and an optical spectrum analyzer (OSA) is used to record the spectrum at the nanowire's output (Fig. 2).

Table 1. Wavelength Listing of Pump, Probe, and Idler Settings for the First Wavelength Conversion Experiment

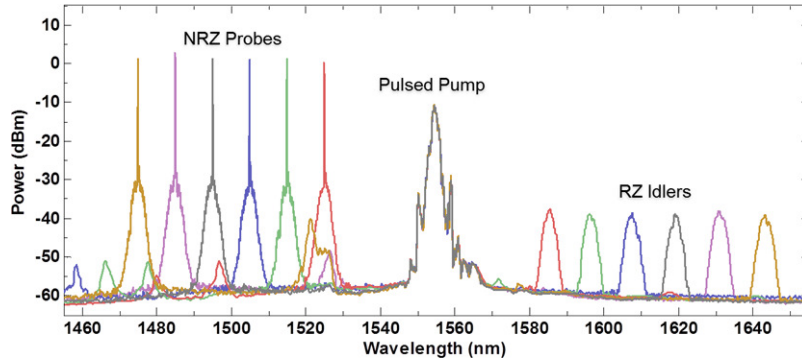|	Wavelength [nm]					
Pump	1555					
Probe	1525	1515	1505	1495	1485	1475
Idler	1585	1596	1607	1619	1631	1643
Separation	60	81	102	124	146	168

Fig. 2. Overlaid spectra of wavelength conversion experiments recorded at the chip output, depicting conversion of 60 nm up to 168 nm. Beyond generated idlers, additional FWM products are visible at shorter wavelengths (1497 nm, 1478 nm, 1459 nm) corresponding to FWM in which two probe photons interact with a single pump photon. Some residual TDFA noise is also visible (1522 nm, 1466 nm).

We validate broadband performance of the device by varying the probe wavelength over the S-band in discrete steps as detailed in Table 1. In this experiment we use a relatively low power 16.5-dBm pump (launched onto the nanowaveguide) which yields a conversion efficiency of ~-32.4 dB (defined here as the off-chip average-powers' ratio between the input probe and the output idler) which is sufficient in order to recover the converted signals while minimizing chip-heating-induced coupling fluctuations. The pump wavelength in this set of measurements is sufficiently close to the ZGVD wavelength to yield near-constant conversion efficiency, which shows the relative flexibility of a single nanowaveguide with regard to pump, probe, and idler wavelengths, as afforded by the flat dispersion profile of the device.
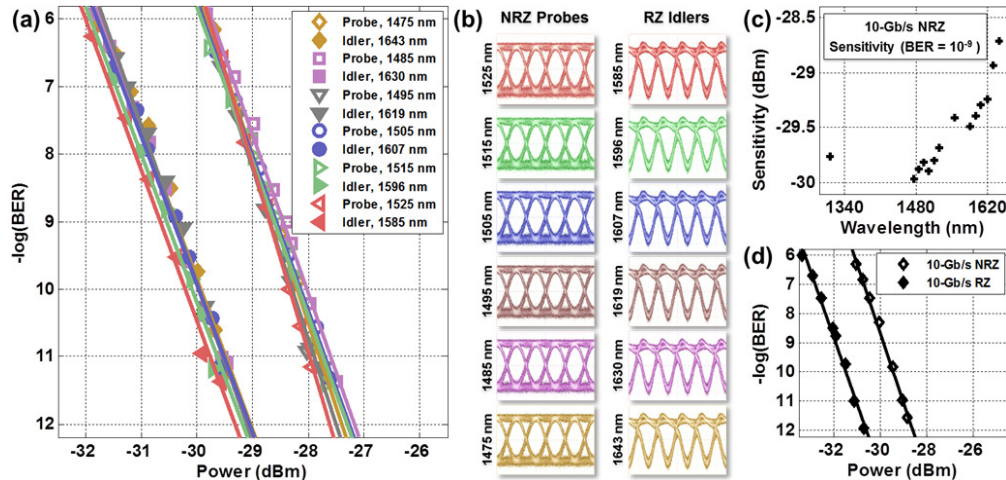

Fig. 3. (a) Recorded BER curves for all probe and idler signals indicating an average 1.9 dB sensitivity gain. (b) Probes' and the idlers' eye diagrams recorded from the inverted-data differential output port of the APD-TIA. (c) Measured APD sensitivity vs. wavelength measured with 10-Gb/s NRZ back-to-back signals. (d) Directly modulated RZ and NRZ back-to-back showing a 2-dB APD sensitivity difference.

Data measurements show open eye diagrams (Fig. 3(b)) on both probe and idler signals. In order to factor out the receiver's wavelength-varying sensitivity from the characterization of the FWM process, we directly measure the receiver's sensitivity at a BER of 10^{-9} versus wavelength using 10-Gb/s NRZ back-to-back signals (Fig. 3(c)). We can then use the difference between the reference sensitivity (set as the C-band value) and the sensitivity at each wavelength as a relative correction factor. Subsequently, each BER curve for the probes

and idlers (Fig. 3(a)) is shifted horizontally by an amount equal to the relevant correction factor in order to deduce the power penalty resulting primarily from FWM. The resulting average sensitivity gain of 1.9 dB is in agreement with previously published results limited to the C-band [25]. The sensitivity gain stems from the NRZ-to-RZ format conversion. This is verified by comparing the receiver's sensitivity to 10-Gb/s modulation of the MLL output (RZ) and a CW TL output (NRZ) showing a 2-dB difference (Fig. 3(d)).

2.3 Wavelength and format conversion at 545-nm probe-idler separation

In order to extend the wavelength conversion range, we modify the experimental setup (Fig. 1(b)) and incorporate an extended cavity laser (ECL) to generate CW light at 1866 nm and a different TDFA providing gain around 1900 nm to boost the probe. We also set the pump wavelength at 1546.5-nm to optimize the conversion bandwidth. Band combiners are used both for combining the pump and probe as well as filtering the idler after the chip. We further suppress the probe after the chip by coiling an optical fiber tightly (~2.5 cm diameter), creating bending losses at the longer wavelength. Since the APD is not sensitive above 1650 nm, the 1866-nm probe is received using a 10-GHz Extended-InGaAs PIN photodetector, while the idler is received using the APD. A 10-GHz communications-signal-analyzer (CSA) is used to record the eye diagrams from the photodetetors' output.
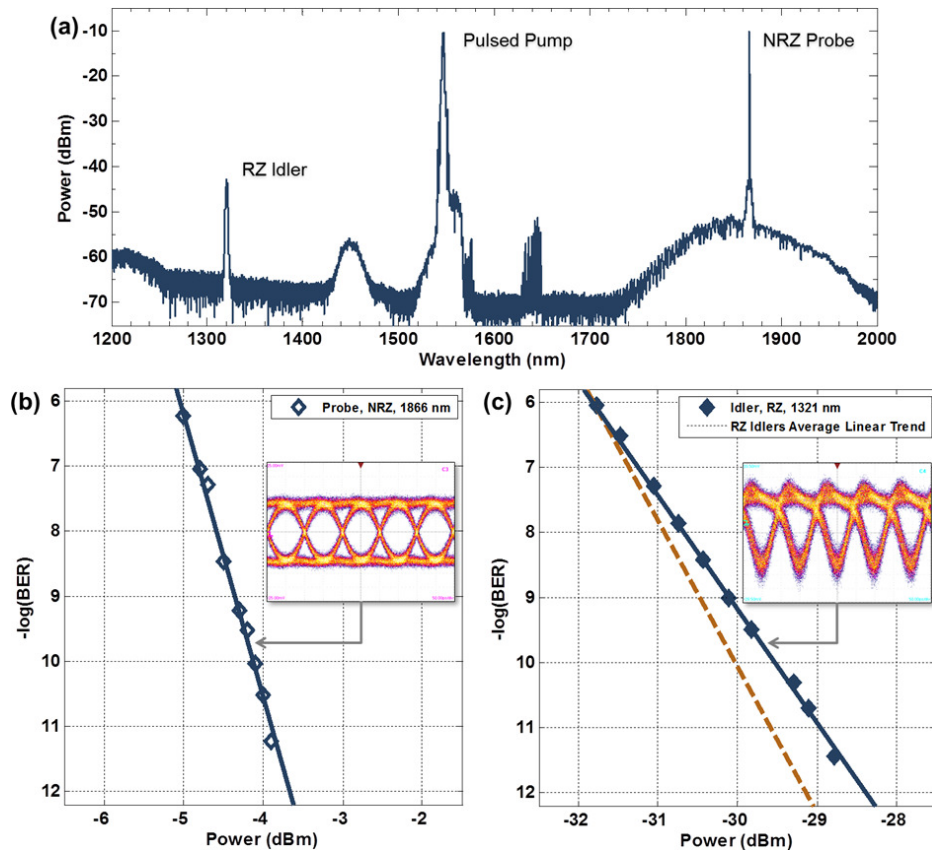

Fig. 4. (a) OSA trace recorded at the chip's output showing wavelength conversion of a 1866-nm probe to a 1321-nm idler. TDFA noise artifacts are visible at 1450 nm, 1640 nm (not fully suppressed TDFA pump), and at the broad gain region around 1850 nm. (b) Probe BER curve recorded using an Extended-InGaAs photodetector (inset of eye diagram recorded on CSA). (c) Idler BER curve recorded on APD receiver (inset of eye diagram) and an average idlers' BER curve based on curves recorded at 1585-nm to 1643-nm. The BER curve has 0.4 dB power penalty compared to the average idlers' curve.

The recorded conversion spectrum (Fig. 4(a)) shows slightly higher conversion efficiency (~-27 dB) in this setup since we inject a higher pump power (19 dBm) to provide sufficient idler power for error-free reception. As before, we observe open eye diagrams (Fig. 4(b), 4(c) insets) on both probe and idler and observe error-free operation for both. In order to characterize the wavelength-converter performance, we compare the idler's BER curve with the average of the idlers' BER curves measured in the previous section (Fig. 3(a)), showing less than a 0.4-dB relative penalty at a BER of 10-9 (as before, the wavelength-dependence of the APD sensitivity is factored out by using the measured correction factors). This relative penalty is attributed to less optimal filtering in this setup.

2.4 Data unicast at 700-nm probe-idler separation

Another FWM-based functionality of interest in optical networks is the multicast operation in which the pump bears data that is imprinted into multiple idlers [21], or alternatively into a single idler (i.e. unicast). In this case, we demonstrate the unicast functionality with a further extended probe-idler separation – set at 700 nm. The experimental setup for this configuration (Fig. 1(c)) includes modulation of the pump with on-off keying data and both pump (in a back-to-back case) and idler are received by the APD-TIA. In this experiment the data originates in RZ format and is maintained as RZ on the idler, but in this case sensitivity gain is expected because of signal regeneration through the FWM process [20].
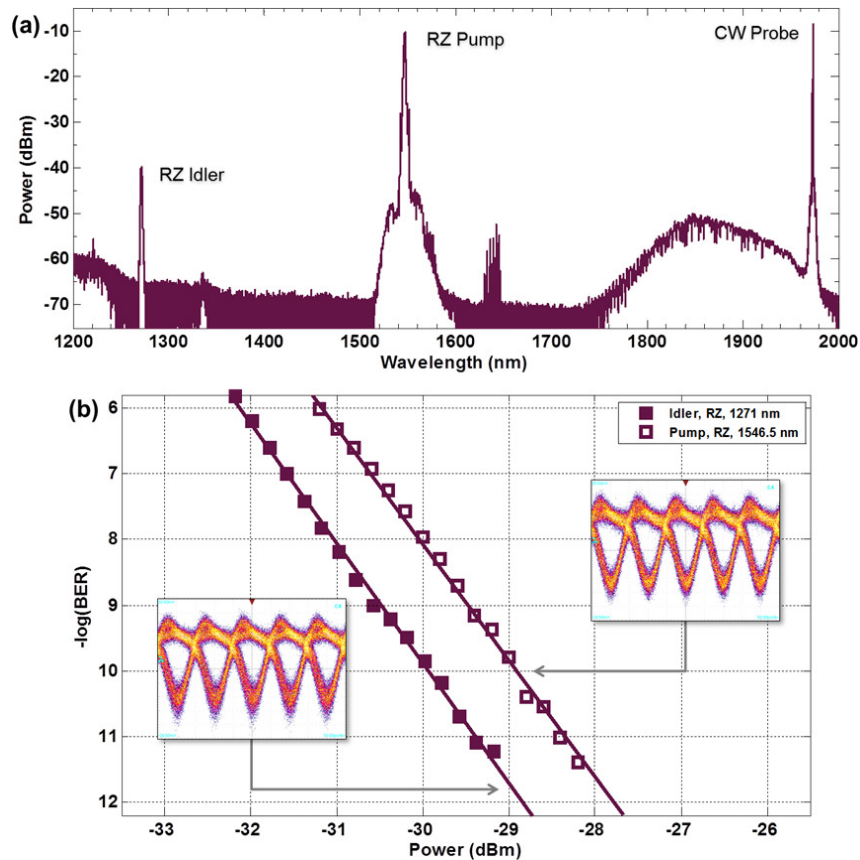

Fig. 5. (a) OSA trace recorded at the chip's output showing data unicast with a CW 1973-nm probe and a RZ 1271-nm idler. TDFA noise artifacts are now visible at ~1640 nm (not fully suppressed TDFA pump), and at the broad gain region around 1850 nm. (b) BER curv es recorded for the 10-Gb/s modulated pump before injection into the silicon chip, and the 10-Gb/s generated idler. Eye diagrams for all signals are included as insets.

The recorded conversion spectrum (Fig. 5(a)) at this setting shows similar conversion efficiency compared to the second experiment. We observe open eye diagrams (Fig. 5(b) insets) on both pump and idler RZ-data signals and observe error-free operation for both. We record the pump back-to-back eye diagrams and BER curves (Fig. 5(b)) just before it is launched on the chip. After the chip we measure the idler's BER curve to have a sensitivity gain of 1 dB which is attributed to the modulation extinction ratio improvement that results from the quadratic pump-idler amplitude relation. As before, the APD wavelength-dependent sensitivity is adjusted for using the computed correction factor (we use the factor measured at 1312 nm since we could not directly measure the sensitivity at 1271 nm). To the best of our knowledge, this is the first reported demonstration of a unicast across such large probe-idler separations in silicon.

3. Summary and conclusions

In this work we have validated the silicon platform's capability for all-optical processing of data at record probe-idler separations within a continuous 3-dB bandwidth. Wavelength conversion was demonstrated to have near constant performance, with consistent sensitivity gains at all probe-idler settings, scaling even up to a record 545-nm separation. Furthermore, we have demonstrated a unicast functionality of high-speed data with a sensitivity gain at even greater probe-idler separation of 700 nm, which shows the device's flexibility for data manipulation with exceedingly large spectral range at our disposal using a single device.

Beyond data-validating the spectral bandwidth of the device for potential usage from 1300 to 2000 nm, it bears noting that these demonstrations also showcase the silicon's potential to perform all-optical processing with relatively low powers (< 100 mW launched on chip) and an ultra-compact footprint (< 1 mm^2), allowing potential integration into compact low power devices. In an era where both power consumption and size become limiting factors for many real-world systems, such advantages might come into play as silicon nonlinear devices develop into commercial components.

Acknowledgments